Journal of Power Electronics (2021) 21:693–702
https://doi.org/10.1007/s43236-021-00217-9

ORIGINAL ARTICLE

Rotor position estimation over entire speed range of interior permanent magnet synchronous motors

Hyung-Woo Lee[1] · **Dae-Hyun Cho**[1] · **Kyo-Beum Lee**[1]

Received: 5 November 2020 / Revised: 31 December 2020 / Accepted: 4 January 2021 / Published online: 2 February 2021

Abstract
This paper presents a method for transitioning between sensorless rotor position estimation methods for an interior permanent magnet synchronous motor (IPMSM). Through the proposed method, rotor position estimation over the entire speed range of the IPMSM is possible. Considering that each sensorless method governs a different speed range for estimating rotor position and speed with good accuracy, a strategy for transitioning between two methods is indispensable. In this study, a sensorless method based on extended back electromotive force (EMF) is used for high-speed operation. In addition, during low-speed operation, rotor position is estimated using the slope of measured current through the application of a zero-voltage vector. A weight function is applied to the position and speed information obtained from the two sensorless methods. The combined information is then used throughout the speed range of the IPMSM. To achieve smooth transitions, the weight function is altered based on the rotor speed in the transition region. The effectiveness of the proposed transition method was demonstrated via simulations and experiments.

Keywords Interior permanent magnet synchronous motor · Sensorless control · Extended electromotive force · Zero-voltage vector · Transition method

1 Introduction

Interior permanent magnet synchronous motors (IPMSMs) feature a permanent magnet inside a rotor, which enables high efficiency and prevents losses during flux generation. Owing to their fast response and high torque density relative to their weight, IPMSMs have been widely employed in high-performance motor drives that require instantaneous torque control [1–8]. Instantaneous torque control in IPMSMs can be achieved using field-oriented control. However, this approach also requires information such as rotor position and speed. To obtain this information, conventionally, a position sensor, such as an encoder or a resolver, is mounted on the shaft of the motor. However, the use of such sensors requires additional expenses, space, and continuous maintenance of the system. Thus, several rotor position and speed estimation methods have been proposed to address these issues [9–12].

✉ Kyo-Beum Lee
kyl@ajou.ac.kr

[1] Department of Electrical and Computer Engineering, Ajou University, Suwon, Korea

During medium-speed and high-speed operations of an IPMSM, an estimation method based on the extended back electromotive force (EMF) is typically used [13–16]. This sensorless method, which is based on the extended EMF, involves a simple estimation procedure and fewer calculations. However, at low speeds, the estimation accuracy afforded by this method decreases, since the EMF of the motor reduces proportionally to the speed of the rotor.

Various sensorless methods have been suggested to overcome this limitation of methods based on the extended EMF in low speed ranges. Among these, methods based on high-frequency signal injection are commonly used [17, 18]. In these methods, a high-frequency signal is injected into the output of the current controller. Then, position and speed information is estimated by processing the signal of the high-frequency component generated by the motor [19, 20]. This method achieves a higher estimation performance in low speed ranges, when compared to methods based on the extended EMF. However, the injection of high-frequency components causes ripples in the output current, which results in ripples in the output torque of the motor. The ripples in the output torque cause additional noise and high-frequency loss during operation [21]. To overcome this

limitation, methods based on the zero-voltage vector were proposed in [22–24]. These methods estimate the position and speed information of the rotor under the application of a zero-voltage vector. During the application of this vector, the slope of the stator current is employed to calculate the rotor position.

This paper proposes a strategy for transitioning between two different sensorless methods. Sensorless control schemes based on an extended EMF and a zero-voltage vector are used for the operation of an IPMSM over its entire speed range. In low speed ranges, a method based on zero-voltage vectors is employed to estimate the rotor position. On the other hand, during medium-speed and high-speed operation, the rotor position is calculated using a method based on an extended EMF. A weight function is applied to the information estimated via each of the sensorless methods to ensure a smooth transition. To demonstrate the effectiveness of the proposed method, simulation and experiments have been conducted.

2 Sensorless control methods for IPMSMs

2.1 Basic modeling of an IPMSM

Figure 1 shows a space vector diagram of an IPMSM. The α–β axes, according to the stationary reference frame, are fixed to the stator. The d–q axes form the synchronous reference frame, which is synchronized with the rotor position θ_r. The d axis corresponds to the north pole of the permanent magnet. The γ–δ frame, synchronized with the estimated rotor position, is the synchronous reference frame estimated using the extended EMF method. It has a position error of $\tilde{\theta}_{EEMF}$ and $\hat{\theta}_{EEMF}$ relative to the d–q and the α–β axes, respectively.

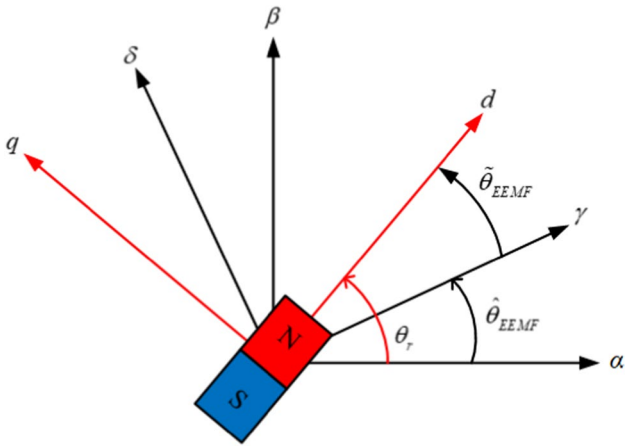

Fig. 1 Space vector diagram of an IPMSM

On rotating the reference frame of the d–q axes, the voltage equation of an IPMSM is described as:

$$\begin{bmatrix} v_d \\ v_q \end{bmatrix} = \begin{bmatrix} R_s + pL_d & -\omega_r L_q \\ \omega_r L_d & R_s + pL_q \end{bmatrix} \begin{bmatrix} i_d \\ i_q \end{bmatrix} + \begin{bmatrix} 0 \\ \omega_r \phi_f \end{bmatrix} \tag{1}$$

where L_d and L_q are the inductances along the rotating d–q axes, ω_r is the rotor speed, and ϕ_f is the flux linkage. p and R_s represent the differential operator and the resistance of the stator, v_d and v_q are the stator input voltages along the rotating d–q axes, and i_d and i_q are the stator currents along the rotating d–q axes. By transforming Eq. (1) from the rotating frame to the stationary frame, the voltage equation for the α–β axes can be expressed as:

$$\begin{bmatrix} v_\alpha \\ v_\beta \end{bmatrix} = \begin{bmatrix} R_s + p(L_1 + L_2 \cos 2\theta_r) & pL_2 \sin 2\theta_r \\ pL_2 \sin 2\theta_r & R_s + p(L_2 - L_1 \cos 2\theta_r) \end{bmatrix} \begin{bmatrix} i_\alpha \\ i_\beta \end{bmatrix} + \omega_r \phi_f \begin{bmatrix} -\sin\theta_r \\ \cos\theta_r \end{bmatrix} \tag{2}$$

where v_α and v_β are the voltages and i_α and i_β are the currents along the α–β axes. In addition, $L_1 = (L_d + L_q)/2$, and $L_2 = (L_d - L_q)/2$.

2.2 Extended EMF method

The method based on an extended EMF calculates the rotor position and speed considering the direct proportionality between the EMF and the rotor speed. This method involves a simple procedure and fewer calculations, when compared to other estimation methods.

Assuming that the difference between L_d and L_q is sufficiently small, Eq. (1) can be described as:

$$\begin{bmatrix} v_d \\ v_q \end{bmatrix} = \begin{bmatrix} R_s + pL_q & -\omega_r L_d \\ \omega_r L_d & R_s + pL_q \end{bmatrix} \begin{bmatrix} i_d \\ i_q \end{bmatrix} + \begin{bmatrix} 0 \\ e_{EEMF} \end{bmatrix}$$
$$e_{EEMF} = \omega_r \left[(L_d - L_q) i_d + \phi_f \right] - (L_d - L_q) p i_q \tag{3}$$

where e_{EEMF} is an extended EMF represented on the d–q axes.

When transforming Eq. (3) from the rotating reference d–q frame to the estimated α–β frame, the voltage equation on the γ–δ frame is expressed as:

$$\begin{bmatrix} v_\gamma \\ v_\delta \end{bmatrix} = \begin{bmatrix} R_s + pL_d & -\omega_r L_q \\ \omega_r L_q & R_s + pL_d \end{bmatrix} \begin{bmatrix} i_\gamma \\ i_\delta \end{bmatrix} + \begin{bmatrix} e_\gamma \\ e_\delta \end{bmatrix}$$
$$\begin{bmatrix} e_\gamma \\ e_\delta \end{bmatrix} = e_{EEMF} \begin{bmatrix} -\sin\tilde{\theta}_{EEMF} \\ \cos\tilde{\theta}_{EEMF} \end{bmatrix} + \left(\hat{\omega}_{EEMF} - \omega_r \right) \begin{bmatrix} -i_\delta \\ i_\gamma \end{bmatrix} \tag{4}$$

where e_γ and e_δ denote the extended EMFs represented on the γ–δ axes, $\hat{\omega}_{EEMF}$ is the estimated speed using the extended EMF method, and ω_r is the speed of the rotor. The extended EMFs, e_γ and e_δ, are estimated by a least order observer. Assuming that the error between the estimated speed, $\hat{\omega}_{EEMF}$, and the actual speed, ω_r, is sufficiently small, the correlation between the estimated extended EMF and the position error of the γ–δ axes, $\tilde{\theta}_{EEMF}$, can be described as:

$$\begin{bmatrix} \hat{e}_\gamma \\ \hat{e}_\delta \end{bmatrix} = e_{EEMF} \begin{bmatrix} -\sin\tilde{\theta}_{EEMF} \\ \cos\tilde{\theta}_{EEMF} \end{bmatrix}, \ \tilde{\theta}_{EEMF} = \tan^{-1}\left(-\frac{\hat{e}_\gamma}{\hat{e}_\delta}\right). \quad (5)$$

The value of $\tilde{\theta}_{EEMF}$, obtained from Eq. (5), is used to estimate the rotor position using the position-speed estimator. A proportional-integral (PI) controller is used to obtain the estimated speed, $\hat{\omega}_o$. Then, by integrating this estimated value, the position of $\hat{\theta}_{EEMF}$ is obtained. The estimated speed, $\hat{\omega}_{EEMF}$, used for the actual control of the IPMSM is obtained by applying a low-pass filter to $\hat{\omega}_o$. Figure 2 depicts a block diagram of the position and speed estimation algorithm based on an extended EMF.

2.3 Zero-voltage vector method

A sensorless method based on a zero-voltage vector measures the slope of the stator current when the zero-voltage vector is applied to the stator. Under this condition, the implied voltage to the stator is null. Therefore, Eq. (2), with the voltage equation on the stationary reference frame, can be rewritten as:

$$\begin{aligned} M_L \cdot p\begin{bmatrix} i_\alpha \\ i_\beta \end{bmatrix} &= -R_s\begin{bmatrix} i_\alpha \\ i_\beta \end{bmatrix} - \phi_f\omega_r\begin{bmatrix} -\sin\theta_r \\ \cos\theta_r \end{bmatrix} \\ &\quad -\omega_r\begin{bmatrix} -2L_2\sin 2\theta_r & 2L_2\sin 2\theta_r \\ 2L_2\cos 2\theta_r & 2L_2\cos 2\theta_r \end{bmatrix}\begin{bmatrix} i_\alpha \\ i_\beta \end{bmatrix} \end{aligned} \quad (6)$$

Where the inductance matrix, M_L, is represented in terms of the inductance and rotor position as:

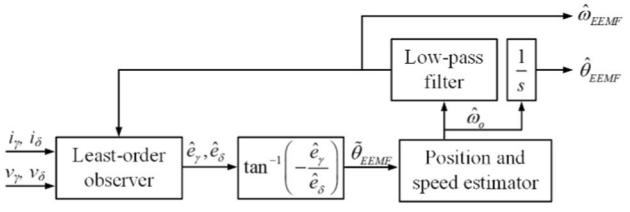

Fig. 2 Block diagram of a position and speed estimation algorithm based on an extended EMF

$$M_L = \begin{bmatrix} L_1 + L_2\cos 2\theta_r & L_2\sin 2\theta_r \\ L_2\sin 2\theta_r & L_1 - L_2\cos 2\theta_r \end{bmatrix} \quad (7)$$

By multiplying the inverse matrix of M_L on both side of Eq. (6), the equation can be rewritten as:

$$\begin{aligned} \frac{di_\alpha}{dt} &= \frac{1}{L_dL_q}\{2L_1L_2\sin 2\theta_r - R_s(L_1 - L_2\cos 2\theta_r)i_\alpha\} \\ &\quad -\frac{2L_2}{L_dL_q}(L_1\omega_r\cos 2\theta_r - 2L_2\omega_r - R_s\sin 2\theta_r)i_\beta \\ &\quad +\frac{\phi_f\omega_r}{L_q}\sin\theta_r \\ \frac{di_\beta}{dt} &= \frac{2L_2}{L_dL_q}\{(R_s\sin 2\theta_r - L_1\omega_r\cos 2\theta_r - 2L_2\omega_r)i_\alpha\} \\ &\quad -\frac{1}{L_dL_q}\{-R_s(L_1 + L_2\cos 2\theta_r) + 2L_1L_2\omega_r\sin 2\theta_r i_\beta\} \\ &\quad -\frac{\phi_f\omega_r}{L_q}\cos\theta_r \end{aligned} \quad (8)$$

Where $\hat{\theta}_z$ is the estimated position calculated using the zero-voltage vector method. Multiply $\sin\hat{\theta}_z$ with the terms reflected on the α axis, and multiply $\cos\hat{\theta}_z$ with the terms reflected on the β axis. Then, the subtraction of these two equations yields:

$$\begin{aligned} &\frac{di_\alpha}{dt}\sin\hat{\theta}_z - \frac{di_\beta}{dt}\cos\hat{\theta}_z \\ &= \frac{1}{L_dL_q}\{2L_1L_2cos(2\theta_r - \hat{\theta}_z)i_\alpha - R_s(L_1\sin\hat{\theta}_z + L_2\cos(2\theta_r - \hat{\theta}_z))i_\alpha \\ &\quad +R_s(L_1\cos\hat{\theta}_z + L_2\sin(2\theta_r - \hat{\theta}_z))i_\beta + 2L_1L_2\omega_r\sin(2\theta_r - \hat{\theta}_z)i_\beta \\ &\quad +2L_2^2\omega_r(i_\alpha\cos\hat{\theta}_z + i_\beta\sin\hat{\theta}_z)\} + \frac{\phi_f\omega_r}{L_q}\cos(\theta_r - \hat{\theta}_z). \end{aligned} \quad (9)$$

Assuming that the position error of the estimated $\hat{d} - \hat{q}$ axes is sufficiently small, according to the Taylor expansion, the following approximation is validated.

$$\begin{aligned} \cos(\hat{\theta}_z + 2\tilde{\theta}_z) &= \cos\hat{\theta}_z - \frac{1}{2!}(2\tilde{\theta}_z)^2 + o(\tilde{\theta}_z^2) \cong \cos\hat{\theta}_z \\ \sin(\hat{\theta}_z + 2\tilde{\theta}_z) &= \sin\hat{\theta}_z + 2\tilde{\theta}_z + o(\tilde{\theta}_z) \cong \sin\hat{\theta}_z \end{aligned} \quad (10)$$

where $\tilde{\theta}_z$ is the position error between the actual position θ_r and the estimated position $\hat{\theta}_z$.

By applying the approximation of Eq. (10), Eq. (9) is rewritten as:

$$L_q\left(\frac{di_\alpha}{dt}\sin\hat{\theta}_z-\frac{di_\beta}{dt}\cos\hat{\theta}_z\right)=R_s\left(i_\beta\cos\hat{\theta}_z-i_\alpha\sin\hat{\theta}_z\right)+2L_2\left(i_\alpha\cos\hat{\theta}_z+i_\beta\sin\hat{\theta}_z\right)\omega_r+\phi_r\omega_r. \quad (11)$$

The second term on the right side can be approximately regarded as the current along the d axis, and the actual speed in the equation, ω_r, can be replaced by the estimated speed, which is the derivative term of the estimated rotor position. Therefore, Eq. (11) can be simplified as:

$$\frac{d\hat{\theta}_z}{dt}=\frac{L_q}{\phi_f}\left\{\left(\frac{di_\alpha}{dt}+\frac{R}{L_q}i_\alpha\right)\sin\hat{\theta}_z-\left(\frac{di_\beta}{dt}+\frac{R}{L_q}i_\beta\right)\cos\hat{\theta}_z\right\}. \quad (12)$$

Using Eq. (12), the estimated speed can be calculated, and the estimated position can be calculated by integrating the estimated speed. Figure 3 shows a block diagram of the position and speed estimation algorithm based on the zero-voltage vector.

3 Proposed transition method

A sensorless control method based on an extended EMF, owing to its simple calculation, is commonly used for the high-speed operation of IPMSMs. However, during low-speed operation, the EMF of the motor decreases with the speed. Therefore, the estimation accuracy of this method decreases. Similarly, a method based on a zero-voltage vector, which enables less audible noise than the high-frequency injection method, suffers from decreased estimation accuracy during the high-speed operation of IPMSMs, where the application time for the zero-voltage vector is reduced.

As stated previously, estimation methods based on an extended EMF and a zero-voltage vector have different rated regions. Considering this, in the proposed scheme, methods based on an extended EMF and a zero-voltage vector are used to complement each other. Thus, a strategy for the sensorless operation of IPMSMs over their entire speed range is presented.

To realize sensorless control over the entire speed range of an IPMSM, several methods for transitioning between two different rotor position estimation strategies have been proposed. Among these, a typical approach is to select a transition point based on the rotor position errors of the two sensorless schemes [25–27]. However, position errors can differ depending on variations in the parameters of the motor and the load. As a result, the transition region also varies. To address this, a weight function is proposed to ensure smooth transitions between the sensorless control methods. In previous transition schemes, a weight function was applied to either the position information or the speed information [28, 29]. However, when a transition occurs at a constant speed, the estimation accuracy decreases owing to the accumulation of position errors from both of the sensorless methods, due to the estimated speed applied in the transition region. Therefore, in the proposed transition strategy, the weight function is applied to the position information and the speed information from each of the sensorless methods. The combined position and speed information is then used to determine the transition region.

In the proposed strategy for transitioning between two sensorless control methods, the rotor position is calculated using each of the sensorless methods. Figure 4 shows the weight function for of the each sensorless methods depending on the rotor speed, where $f(n)$ and $1\text{-}f(n)$ are the weight functions of methods based on an extended EMF and a zero-voltage vector, respectively. The weight function is applied to the position and speed information, which is represented as:

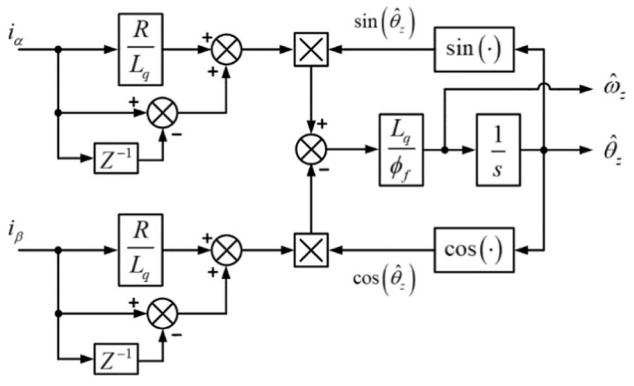

Fig. 3 Block diagram of a position and speed estimation algorithm based on a zero-voltage vector

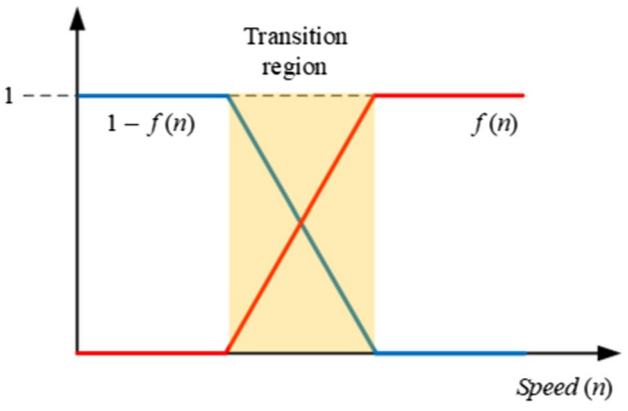

Fig. 4 Weight function for each of the sensorless methods according to rotor speed

$$\hat{\theta}_r = \hat{\theta}_z \times \{1 - f(n)\} + \hat{\theta}_{EEMF} \times f(n)$$
$$\hat{\omega}_r = \hat{\omega}_z \times \{1 - f(n)\} + \hat{\omega}_{EEMF} \times f(n) \quad (13)$$

where $\hat{\theta}_r$ and $\hat{\omega}_r$ are the position and speed over the entire speed range of the motor, which are estimated by a combination of the sensorless methods. In Eq. (13), the weight function is applied to the position and speed information from each of the methods to obtain the estimated position and speed of the transition range. When the rotor speed increases from low to high speeds, the weight function of the extended EMF method *f(n)* has values of 0 and 1 before and after the transition region, respectively. Furthermore, the weight function of the zero-voltage vector method is represented by subtracting *f(n)* from 1. Therefore, during low-speed operation, the IPMSM is controlled by information calculated using the zero-voltage vector method. For transitioning to the second sensorless method during medium-speed operation, the transition region is determined based on speed.

To simplify the implementation and to prevent rapid fluctuations of the information used in the control, the value of the weight function is changed into a linear form with a constant slope within the transition region. When the rotor speed increases, the weight function of the extended EMF method increases linearly until it reaches the value of 1. Therefore, at the end of the transition region, the IPMSM is controlled by the method based on the extended EMF.

The point at which the transition of the control scheme begins to change is determined by considering the number of consecutive zero-voltage vectors applied. Figure 5 shows the minimum requirements for employing the method based on the zero-voltage vector. In the sensorless method based on the zero-voltage vector, the slope of the stator current can be calculated when at least two consecutive zero-voltage vectors are applied. This implies that the amount of time the zero-voltage vector is applied to the motor should be greater than twice the control period, T_s. As stated previously, the amount of time the zero-voltage vector is applied decreases when the speed of the IPMSM increases. The transition region should not include the range where the zero-voltage vector is applied less than two consecutive times. This point can vary according to the specifications of the sensor, the micro control unit, and the motor.

Figure 6 shows a block diagram of the application of the weight function, and displays the process of calculating the position and speed information.

Figure 7 presents a block diagram of the rotor position estimation method over the entire speed range of an IPMSM, i.e., the proposed transition strategy. The rotor position is calculated using each of the sensorless methods for the entire speed range. The estimated position used for the speed control of the IPMSM is obtained from sensorless algorithms based on the weight function.

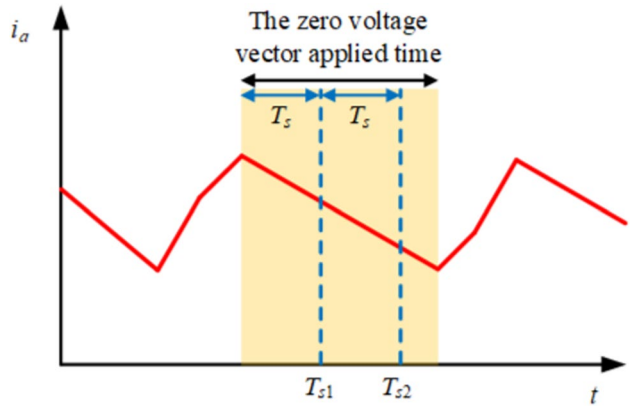

Fig. 5 Minimum condition for operating a zero-voltage vector method

4 Simulation results

The proposed transition strategy was verified using a simulation model. Table 1 lists the parameters of the IPMSM used in this simulation.

Figure 8 shows simulation results of rotor position estimation during low-speed operation. It also depicts the estimated position and speed calculated using the method based on the extended EMF and that based on the zero-voltage

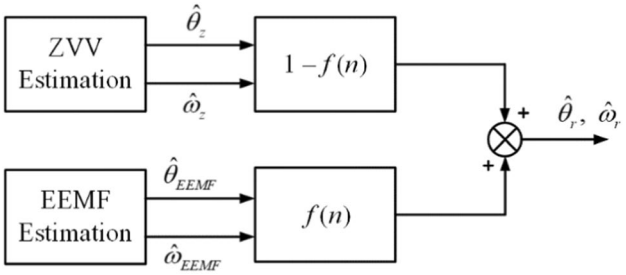

Fig. 6 Block diagram of the application of a weight function

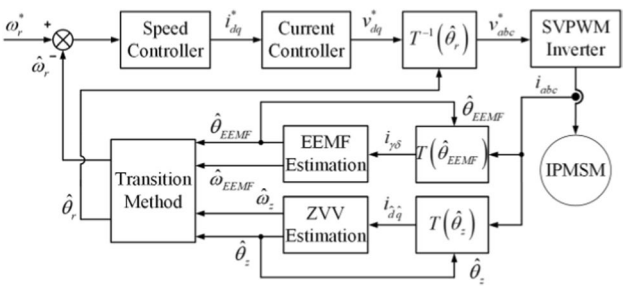

Fig. 7 Block diagram of the proposed transition method

Table 1 IPMSM parameters

Parameters	Value	Unit
Rated power	11	kW
Rated speed	1750	rpm
Stator resistance (R_s)	0.349	Ω
d-axis inductance (L_d)	13.17	mH
q-axis inductance (L_q)	15.60	mH
Permanent magnet flux (ϕ_f)	0.554	Wb
Number of poles (P)	6	–

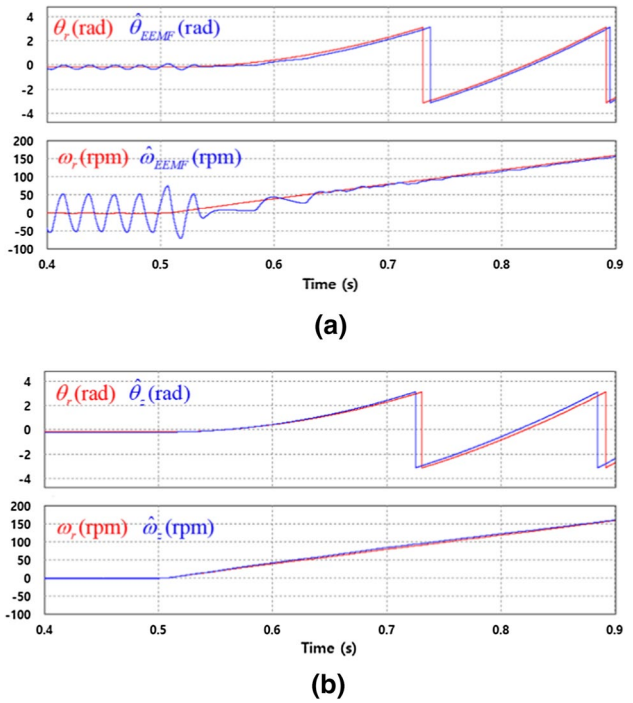

Fig. 8 Simulation results of rotor position estimation during low-speed operation: **a** extended EMF method; **b** zero-voltage vector method

vector. The IPMSM is controlled by information obtained by sensor when the sensorless methods calculate the position of the rotor. The speed of the IPMSM was increased starting from 0 rpm. Figure 8a indicates the estimation performance of the method based on the extended EMF. When the EMF during low-speed operation is significantly weak, the estimation accuracy of this method is low. On the other hand, as shown in Fig. 8b, the zero-voltage vector method can precisely estimate the position and speed, owing to the high ratio of the zero-voltage vector applied to the IPMSM.

Figure 9 shows simulation results of the rotor position estimation during high-speed operation. Similar to Fig. 8, the rotor position and speed calculated via each of the sensorless methods are compared to the results obtained by the sensor. Figure 9a indicates the estimation accuracy of

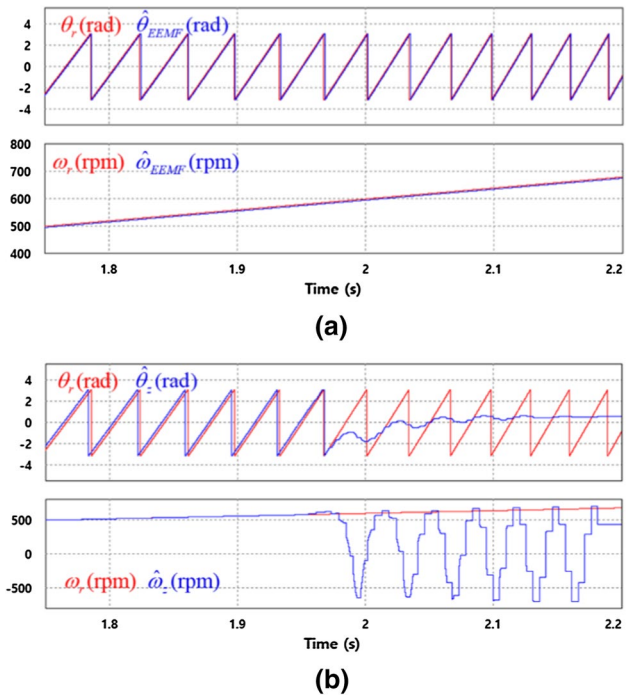

Fig. 9 Simulation results of rotor position estimation during high-speed operation: **a** extended EMF method; **b** zero-voltage vector method

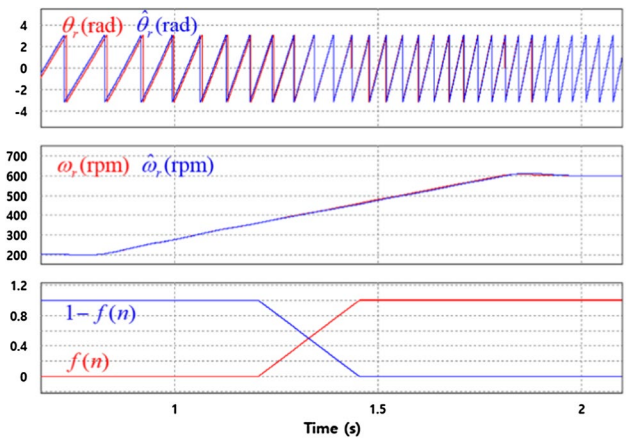

Fig. 10 Simulation results of the proposed transition method

the method based on the extended EMF during high-speed operation, where the speed is increased from 500 rpm. When the rotor speed and EMF are sufficiently high, the estimation performance of the method remains stable. However, as shown in Fig. 9b, the performance of the method based on the zero-voltage vector decreases during high-speed operation, since the length of time the vector is applied decreases as the rotor speed increases.

Figure 10 shows simulation results of the proposed transition method. The speed of the IPMSM was changed from

200 to 600 rpm, under a 15% rated load torque. The estimation method was changed between 350 and 450 rpm. The weight function of the method based on the extended EMF increased from 0 to 1 when the speed of the rotor increased through the transition region. Simultaneously, the weight function of the method based on the zero-voltage vector was reduced from 1 to 0 during this transition range. Thus, through a transition between the control methods, the IPMSM could be operated from the low speed to medium speed ranges.

Figure 11 shows simulation results of the proposed position estimation strategy over the entire speed range. A torque load of 10 Nm was applied, which is 15% of the rated torque. The rotor speed was varied from 0 to 1700 rpm in order to verify the effectiveness of the proposed method in all speed ranges.

5 Experimental results

The validity and performance of the proposed transition method for the sensorless operation of an IPMSM have been experimentally investigated. Figure 12 shows the experimental setup, which is composed of a two-level inverter, a control board, and an IPMSM with the load. A TMS320F28335 micro control unit was used in the control board, and the parameters of the IPMSM were the same as those used for the simulation.

Figure 13 shows the flag of the zero-voltage vector condition. This flag has a value of 1 if the zero-voltage vector is applied; otherwise, its value is 0. It is evident that the zero-voltage vector is applied three consecutive times at 450 rpm, and only once at 600 rpm. In this study, the transition region was set as 350–450 rpm, considering the number of times the zero-voltage vector is consecutively applied. Although

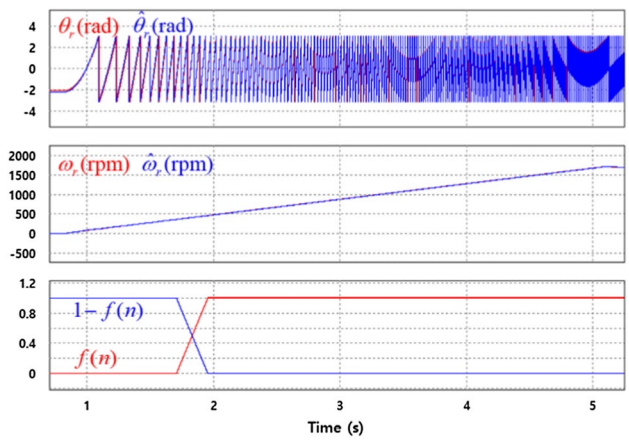

Fig. 11 Simulation results of the proposed position estimation strategy over the entire speed range

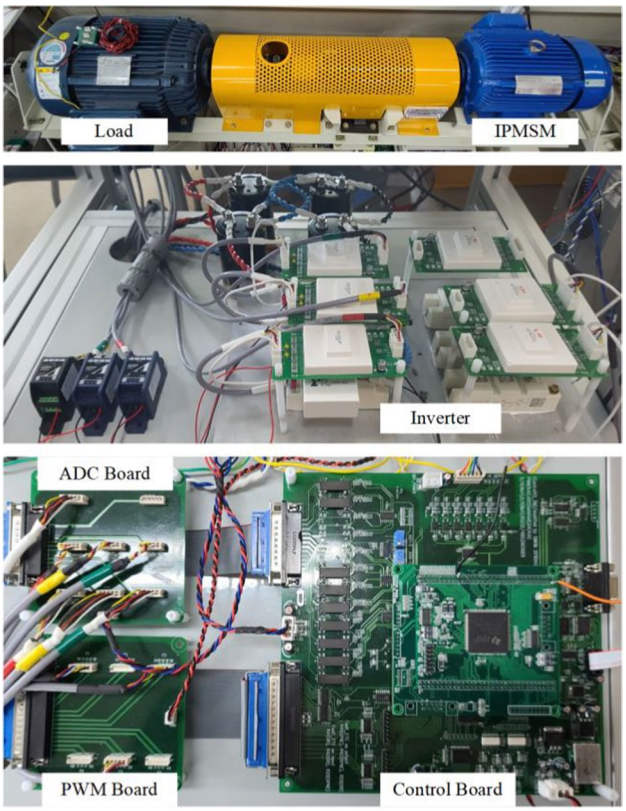

Fig. 12 Experimental setup

the rotor position can be calculated until the zero-voltage vector is consecutively applied twice, the transition region was limited to three consecutive applications of the vector to ensure the accuracy of the estimated information.

Figure 14 shows experimental results of the rotor position estimation depending on the speed of the IPMSM. Through current control of the IPMSM, the reference current of the q axis was fixed at 5 A. The actual position of the rotor, which is used for current control, is measured using an encoder. Figure 14a shows the estimation performance of each of the sensorless methods with respect

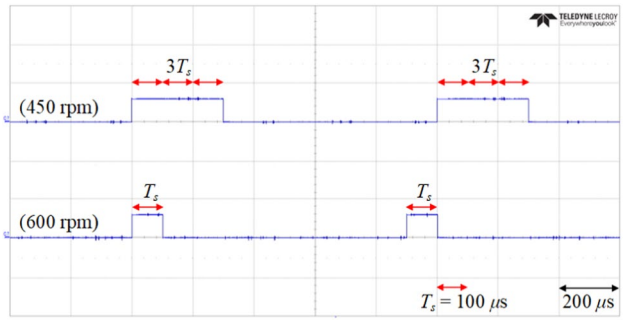

Fig. 13 Flag of the zero-voltage vector condition

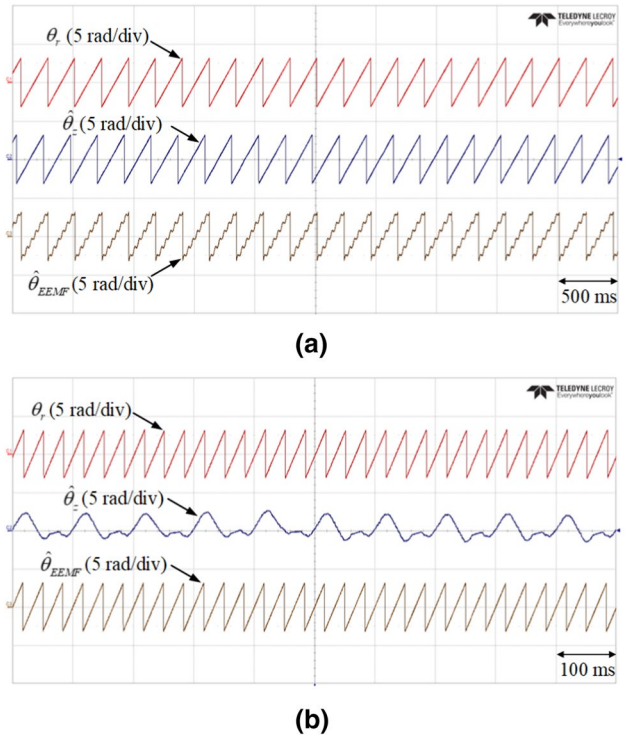

Fig. 14 Experimental results of rotor position estimation depending on the speed of the IPMSM: **a** 90 rpm; **b** 600 rpm

to the actual value. The speed of the rotor was fixed at 90 rpm, where the estimation performance of the method based on the extended EMF was unstable due to a weak EMF. On the other hand, due to the sufficient application of a zero-voltage vector, the position estimation performance of the method based on the zero-voltage vector remained stable.

Figure 14b shows experimental results for the case of medium-speed operation. The speed of the rotor was fixed at 600 rpm. In this figure, the reduced performance of the method based on the zero-voltage vector can be observed. However, the accuracy of the method based on the extended EMF increased, when compared to that during low-speed operation, due to the stronger EMF component.

Figure 15 shows experimental results of the proposed transition method. In this case, the motor speed was varied from 200 to 600 rpm, under the application of 15% of the rated load torque. The transition region was set as 350–450 rpm. In the transition region, the weight function of the extended EMF method, $f(n)$, increased linearly from 0 to 1. By combining the sensorless methods, the control schemes can be smoothly changed. The zero-voltage and extended EMF methods were used for speed control before and after the transition region, respectively. Through the proposed transition method, the IPMSM can be operated in both the low and medium speed ranges.

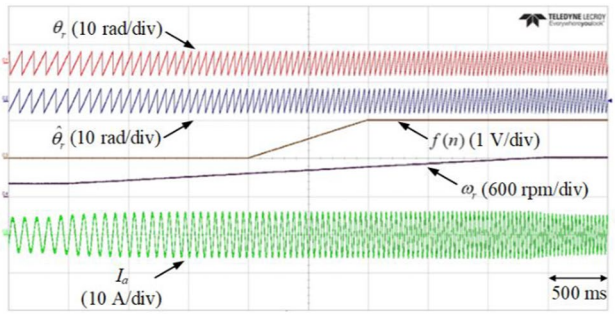

Fig. 15 Experimental results of the proposed transition method

Figure 16 shows experimental results of the proposed position estimation strategy over the entire speed range. The speed was changed from 0 to 1700 rpm to demonstrate the applicability of the proposed method over the entire speed range of the IPMSM, under the application of 15% of the rated load torque.

6 Conclusion

This paper proposes a method for transitioning between two sensorless rotor position estimation methods. Through the proposed method, rotor position estimation over the entire speed range of an IPMSM can be achieved. For position estimation, methods based on the extended EMF and the zero-voltage vector were employed. The estimation method based on the zero-voltage vector was adopted during low-speed operation, while the method based on the extended EMF was adopted during high-speed operation. In the proposed transition method, a weight function was applied to the calculated information (i.e., the position and speed of the rotor) in order to ensure smooth transitions between the two methods. The validity of the proposed transition method was verified via simulations and experiments.

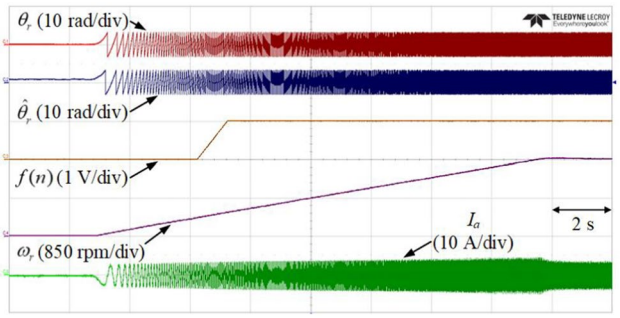

Fig. 16 Experimental results of the proposed position estimation method over the entire speed range

Acknowledgements This research was supported by Korea Electric Power Corporation (Grant No. R19XO01-20) and a grant (20RTRP-B146008-03) from the Railroad Technology Research Program funded by the Ministry of Land, Infrastructure and Transport of the Korean government.

References

1. Lee, K.-B.: PMSM sensorless control. In: Lee, K.-B. (ed.) Advanced Power Electronics, 1st edn., pp. 317–340. Munundang, Seoul (2019)
2. Seo, D.-W., Bak, Y., Lee, K.-B.: An improved rotating restart method for a sensorless permanent magnet synchronous motor drive system using repetitive zero voltage vectors. IEEE Trans Ind Electron **67**(5), 3496–3504 (2020)
3. Cho, Y., Lee, K.-B., Song, J.-H., Lee, Y.I.: Torque-ripple minimization and fast dynamic scheme for torque predictive control of permanent-magnet synchronous motors. IEEE Trans Power Electron **30**(4), 2182–2190 (2015)
4. Bak, Y., Lee, K.-B.: Constant speed control of a permanent-magnet synchronous motor using a reverse matrix converter under variable generator input conditions. IEEE J Emerg Sel Topics Power Electron **6**(1), 315–326 (2018)
5. Cho, D.-H., Bak, Y., Lee, K.-B.: Method of estimating initial rotor position for IPMSMs using subdivided voltage vectors based on inductance variation. J Power Electron **20**(5), 1195–1205 (2020)
6. Chen, Q., Zou, Z.: Lumped-parameter thermal analysis and experimental validation of interior IPMSM for electric vehicle. J. Electr. Eng. Technol. **13**(6), 2276–2283 (2018)
7. Jin, N., Li, G., Zhou, K., Liu, J., Iu, H.H.-C.: MTPA trajectory tracking control with on-line MRAS parameter identification for an IPMSM. J Electr Eng Technol **14**(6), 2355–2366 (2019)
8. Zhang, W., Xiao, F., Liu, J., Mai, Z., Li, C.: Maximum torque per ampere control for IPMSM traction system based on current angle signal injection method. J Electr Eng Technol **15**(4), 1681–1691 (2020)
9. Sul, S.-K., Kwon, Y.-C., Lee, Y.: Sensorless control of IPMSM for last 10 years and next 5 years. CES Trans Elect Mach Syst **1**(2), 91–99 (2017)
10. Lee, K.-G., Lee, J.-S., Lee, K.-B.: Wide-range sensorless control for SPMSM using an improved full-order flux observer. J Power Electron **15**(3), 721–729 (2015)
11. Shen, H., Xu, J., Yu, B., Tang, Q., Chen, B., Lou, C., Qiao, Y.: Seamless transition strategy for wide speed-range sensorless IPMSM drives with a virtual q-axis inductance. J Power Electron **19**(5), 1224–1234 (2019)
12. Hamidani, B., Allag, A., Allag, A., Zeghib, O.: Sensorless nonlinear control applied to a PMSM machine based on new extended MVT observer. J Electr Eng Technol **14**(4), 1615–1623 (2019)
13. Morimoto, S., Kawamoto, K., Sanada, M., Takeda, Y.: Sensorless control strategy for salient-pole PMSM based on extended EMF in rotating reference frame. IEEE Trans Ind Appl **38**(4), 1054–1061 (2002)
14. Lee, Y.-J., Bak, Y., Lee, K.-B.: Restarting method for EEMF based sensorless permanent magnet synchronous motor drive systems. Trans. Korean Inst Power Electr **24**(2), 127–133 (2019)
15. Chen, Z., Tomita, M., Doki, S., Okuma, S.: An extended electromotive force model for sensorless control of interior permanent-magnet synchronous motors. IEEE Trans Ind Electron **50**(2), 288–295 (2003)
16. Han, D.-Y., Cho, Y., Lee, K.-B.: Simple sensorless control of interior permanent magnet synchronous motor using PLL based on extended EMF. J Electr Eng Technol **12**(2), 711–717 (2017)
17. Wang, S., Yang, K., Chen, K.: An improved position-sensorless control method at low speed for PMSM based on high-frequency signal injection into a rotating reference frame. IEEE Access **7**, 86510–86521 (2019)
18. Yoon, T.-M., Lee, J.-S., Lee, K.-B.: Rotor position estimation method of IPMSM using HF signal injection and sliding-mode controller. IEEJ Trans Electr Electron Eng **9**(S1), S56–S63 (2014)
19. Kim, S., Ha, J.-I., Sul, S.-K.: PWM switching frequency signal injection sensorless method in IPMSM. IEEE Trans Ind Appl **48**(5), 1576–1587 (2012)
20. Alaei, A., Lee, D.-H., Ahn, J.-W., Nejad, S.M.S.: Sensorless control of IPMSM with a simplified high- frequency square wave injection method. J Electr Eng Technol **13**(4), 1515–1527 (2018)
21. Wang, G., Yang, L., Yuan, B., Wang, B., Zhang, G., Xu, D., Xu, P., Zhu, Z.Q.: Pseudo-random high-frequency square-wave voltage injection based sensorless control of IPMSM drives for audible noise reduction. IEEE Trans Ind Electron **63**(12), 7423–7433 (2016)
22. Wang, G., Kuang, J., Zhao, N., Zhang, G., Xu, D., Nakashima, S., Inagaki, Y., Miki, I.: Rotor position estimation of PMSM in low-speed region and standstill using zero-voltage vector injection. IEEE Trans Power Electron **33**(9), 7948–7958 (2018)
23. Xu, P.L., Zhu, Z.Q.: Novel carrier signal injection method using zero-sequence voltage for sensorless control of PMSM drives. IEEE Trans Ind Electron **63**(4), 2503–2061 (2016)
24. Xu, P.L., Zhu, Z.Q.: Novel square-wave signal injection method using zero-sequence voltage for sensorless control of PMSM drives. IEEE Trans Ind Electron **63**(12), 7444–7454 (2016)
25. Sim, H.-W., Lee, J.-S., Lee, K.-B.: A simple strategy for sensorless speed control for an IPMSM during startup and over wide speed range. J Electr Eng Technol **9**(5), 1582–1591 (2014)
26. Wang, K., Chen, B., Shen, G., Yao, W., Lee, K.: Online updating of rotor time constant based on combined voltage and current mode flux observer for speed-sensorless AC drives. IEEE Trans Ind Electron **61**(9), 4583–4593 (2014)
27. Han, D.-Y., Yoon, J.-S., Cho, Y., Lee, K.-B., Lee, C.-H., Lee, J.: Improved transition method for sensorless operation of interior permanent magnet synchronous motor drives. Trans Korean Inst Power Electr **65**(8), 1362–1368 (2016)
28. Ide, K., Ha, J.-I., Sawamura, M.: A hybrid speed estimator of flux observer for induction motor drives. IEEE Trans Ind Electron **53**(1), 130–137 (2006)
29. Yang, S.C., Hsu, Y.L.: Full speed range sensorless drive of permanent-magnet machine combining saliency-based and back-EMF-based drive. IEEE Trans Ind Electron **64**(2), 130–137 (2017)

Hyung-Woo Lee received his B.S. degree in Electrical and Computer Engineering from Ajou University, Suwon, Korea, in 2020, where he is presently working towards his M.S. degree in Electrical and Computer Engineering. His current research interests include electric machine drives and power electronics.

Dae-Hyun Cho received his B.S. degree in Electrical and Computer Engineering from Ajou University, Suwon, Korea, in 2019, where he is presently working towards his M.S. degree in Electrical and Computer Engineering. His current research interests include electric machine drives, power electronics, and control systems.

Kyo-Beum Lee received his B.S. and M.S. degrees in Electrical and Electronic Engineering from Ajou University, Suwon, Korea, in 1997 and 1999, respectively. He received his Ph.D. degree in Electrical Engineering from Korea University, Seoul, Korea, in 2003. From 2003 to 2006, he was with the Institute of Energy Technology, Aalborg University, Aalborg, Denmark. From 2006 to 2007, he was with the Division of Electronics and Information Engineering, Jeonbuk National University, Jeonju, Korea. In 2007, he joined the School of Electrical and Computer Engineering, Ajou University. He is an Associate Editor of the IEEE Transactions on Industrial Electronics, the IEEE Transactions on Power Electronics, the Journal of Power Electronics, and the Journal of Electrical Engineering and Technology. His current research interests include electric machine drives, renewable power generation, and electric vehicle applications.